

Singlet and triplet to doublet energy transfer: improving organic light-emitting diodes with radicals

Emrys W. Evans^{2,3+}, Alexander J. Gillett²⁺, Qinying Gu², Junshuai Ding¹, Zhangwu Chen¹, Timothy J. H. Hele⁴, Richard H. Friend^{2*}, Feng Li^{1,2*}

¹*State Key Laboratory of Supramolecular Structure and Materials, College of Chemistry, Jilin University, Qianjin Avenue 2699, Changchun, 130012, P. R. China*

²*Cavendish Laboratory, University of Cambridge, JJ Thomson Avenue, Cambridge, CB3 0HE, United Kingdom*

³*Department of Chemistry, Swansea University, Singleton Park, Swansea, SA2 8PP, United Kingdom*

⁴*Department of Chemistry, University College London, Christopher Ingold Building, London, WC1H 0AJ, United Kingdom*

⁺denotes equal contribution

*e-mail correspondence to: rhf10@cam.ac.uk (RHF), lifeng01@jlu.edu.cn (FL)

Abstract

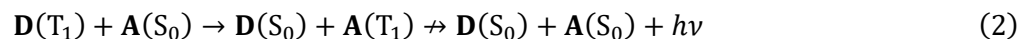
Organic light-emitting diodes (OLEDs) must be engineered to circumvent the efficiency limit imposed by the 3:1 ratio of triplet to singlet exciton formation following electron-hole capture. Here we show the spin nature of luminescent radicals such as TTM-3PCz allows direct energy harvesting from both singlet and triplet excitons through energy transfer, with subsequent rapid and efficient light emission from the doublet excitons. This is demonstrated with a model Thermally-Activated Delayed Fluorescence (TADF) organic semiconductor, 4CzIPN, where reverse intersystem crossing from triplets is characteristically slow (50% emission by 1 μ s). The radical:TADF combination shows much faster emission via the doublet channel (80% emission by 100 ns) than the comparable TADF-only system, and sustains higher electroluminescent efficiency with increasing current density than a radical-only device. By unlocking energy transfer channels between singlet, triplet and doublet excitons, further technology opportunities are enabled for optoelectronics using organic radicals.

Spin management is an important consideration for organic light-emitting diode (OLED) efficiency in display and lighting technologies. For closed-shell molecules with singlet-spin-0 ground state, spin-statistics with electrical excitation leads to the formation of 25% singlet (spin-0, S_1) and 75% triplet (spin-1, T_1) excitons.^{1,2} In first-generation OLEDs, this results in a maximum electroluminescence (EL) internal quantum efficiency (EQE) of 25% as singlet emission (fluorescence, $S_1 \rightarrow S_0 + h\nu$) is allowed whereas triplet emission (phosphorescence, $T_1 \rightarrow S_0 + h\nu$) is spin-forbidden. In commercial applications, triplet-triplet annihilation- and enhanced phosphorescence-based schemes have been used to obtain efficient luminescence from triplet states.³⁻⁷ Other technologies under development include thermally activated delayed fluorescence (i.e. TADF),⁸⁻¹² where electron donor-acceptor molecular designs promote reduced exchange interaction and minimised S_1 - T_1 energy gap for reverse intersystem crossing (rISC, $T_1 \rightarrow S_1$) and delayed S_1 emission. The TADF electroluminescence mechanism is shown in Fig. 1a.

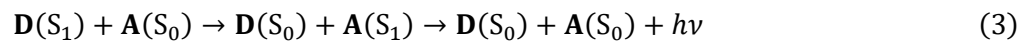
Another possibility to extract emission from the otherwise dark T_1 state is to transfer its energy to another energy acceptor molecule, which then emits light. However, if the acceptor is a ground-state singlet, converting the donor triplet to an acceptor excited-state emissive singlet is spin forbidden:



where $\mathbf{D}(X)$ stands for the energy donor molecule in state X and $\mathbf{A}(X)$ for the energy acceptor, and \rightarrow/\nrightarrow denotes spin allowed/forbidden. It is possible to convert the donor triplet to an acceptor triplet, but emission from this state is spin-forbidden



such that the process converts one dark state to another dark state. A donor singlet can transfer its energy to the acceptor singlet by Förster transfer:

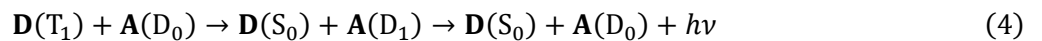


but since this converts one bright state to another bright state, it does not improve the device efficiency, though could improve other device characteristics such as colour purity. Singlet to singlet energy transfer has been achieved, in previous work,¹³⁻¹⁷ where TADF materials have been used as sensitizers in Förster-type energy transfer of TADF S_1 to non-radical fluorescent molecules in a ‘hyperfluorescence’ scheme as depicted in Fig. 1c. In these systems, energy transfer of TADF triplet excitons is indirect and proceeds following reverse intersystem crossing to the TADF S_1 . However, the undesirable triplet-triplet energy transfer to lower energy

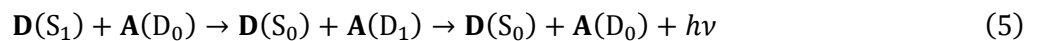
triplets on the ‘hyperfluorescent’ molecule, as mentioned above, as well as undesirable triplet-annihilation interactions, must therefore be suppressed.

In contrast to OLED technologies employing electronic excitations with paired electrons, efficient radical-based OLEDs offer an alternative route to overcoming the spin statistics limit using doublet excitons with spin-allowed doublet emission ($D_1 \rightarrow D_0 + h\nu$ fluorescence), since the dark quartet state Q_1 lies above the D_1 state in energy.^{18–24} The radical OLED photophysical mechanism is shown in Fig. 1b. However, despite demonstrating an excellent peak EQE at low injection current densities, the ‘roll-off’ – decreasing efficiency with increasing current density – is severe in reported radical devices using single-dopant emissive layers where charge trapping directly forms doublet excitons.^{20,25} The role of exciton-exciton and exciton-charge annihilation effects were ruled out by transient PL measurements on electrically-driven OLEDs, leading to the conclusion the charge trapping mechanism for EL must be improved to advance the performance of radical-based devices.²⁵

Here we consider if the desirable properties of radical emitters could be used to ‘brighten’ otherwise dark (or slowly emissive) triplet states where emission efficiency cannot easily be improved by using a ground-state singlet acceptor. In the SI section 1 we show how, using a ground state radical acceptor, triplet energy transfer leading to an emissive excited-state doublet can be quantum mechanically spin-allowed by Dexter transfer:



unlike the case of a ground-state singlet acceptor considered earlier. Energy transfer from an excited-state singlet to a doublet is also allowed via a Förster-type mechanism



meaning that the radicals’ doublet spin nature enables energy harvesting of all electronic excitations in standard organic semiconductors. In addition, rapid EL emission can be enabled in radical energy transfer-based devices, which is desirable: to enhance EL efficiency in OLEDs by outcompeting non-radiative channels, and to avoid building up of high excitation densities at high drive currents that can cause efficiency roll-off. Previously, triplet to doublet energy transfer has been demonstrated in experiments using transient radical acceptors,²⁶ but to the best of our knowledge has not been demonstrated using a stable, emissive radical nor in an optoelectronic device.

We have combined non-radical organic semiconductors as energy donors with radical emitters as energy acceptors to form light-emitting layers. In principle, the strategy we propose can work with a wide range of standard OLED semiconductors so long as their singlet and triplet states are higher in energy than the doublet

exciton in the radical material. It is desirable to choose systems for which the spin exchange energy is kept low, so that the singlet energy is kept low, and (as in the case of ‘hyperfluorescence’ mentioned earlier) we use here TADF materials that are engineered to reduce the exchange energy to thermally accessible values. A further advantage here is that TADF systems undergo rapid intersystem crossing following photoexcitation, allowing us to track singlet and triplet dynamics in transient all-optical measurements. Thus our energy donors and acceptors in double-dopant emissive layers were chosen to be the benchmark TADF material, 1,2,3,5-tetrakis(carbazole-9-yl)-4,6-dicyanobenzene (4CzIPN),⁸ and tris(2,4,6-trichlorophenyl)methyl-3-substituted-9-phenyl-9H-carbazole (TTM-3PCz) radical from our previous work.²⁰ Transient PL (trPL) and absorption (TA) measurements were used to probe the singlet-doublet and triplet-doublet energy transfer mechanisms, showing rapid energy transfer on picosecond and microsecond timescales from singlet and triplet excitons, respectively. Magneto-electroluminescence studies support the role of triplet-doublet energy transfer in radical-based OLEDs. The TADF:radical devices show improved device characteristics, with reduced turn on voltage and roll-off in the EQE, as well as better device stability than single-dopant radical structures. TADF:radical systems extend the spin space of organic optoelectronics, where advantageous ‘hyperfluorescence’ can be retained, dark triplet states removed, and more direct triplet-doublet energy transfer used for efficient radical-based optoelectronics.

Results and Discussion

Radical energy harvesting for doublet emission

Fig. 1d shows an energy level diagram for radical-based OLEDs using double-dopant emissive layers containing non-radical organic components (**D**, energy donor) and radical emitters (**A**, energy acceptor). Singlet (S_1) and triplet (T_1) excitons of **D** can transfer energy to the doublet (D_1)-spin **A** for efficient doublet emission if:

1. The singlet and triplet energy levels of the donor are higher than the D_1 state of the acceptor, i.e. $E(\mathbf{D}, S_1) > E(\mathbf{A}, D_1)$ and $E(\mathbf{D}, T_1) > E(\mathbf{A}, D_1)$ where $E(\mathbf{D}, S_1)$ and $E(\mathbf{D}, T_1)$ are the S_1 and T_1 exciton energies of **D**, and $E(\mathbf{A}, D_1)$ is the radical **A** D_1 exciton energy;
2. The donor-cation/acceptor-anion, $\mathbf{D}^+\mathbf{A}^-$ or donor-anion/acceptor-cation, $\mathbf{D}^-\mathbf{A}^+$ states must be higher energy than the radical D_1 -exciton, i.e. $E(\mathbf{D}^+\mathbf{A}^-) > E(\mathbf{A}, D_1)$ and $E(\mathbf{D}^-\mathbf{A}^+) > E(\mathbf{A}, D_1)$.

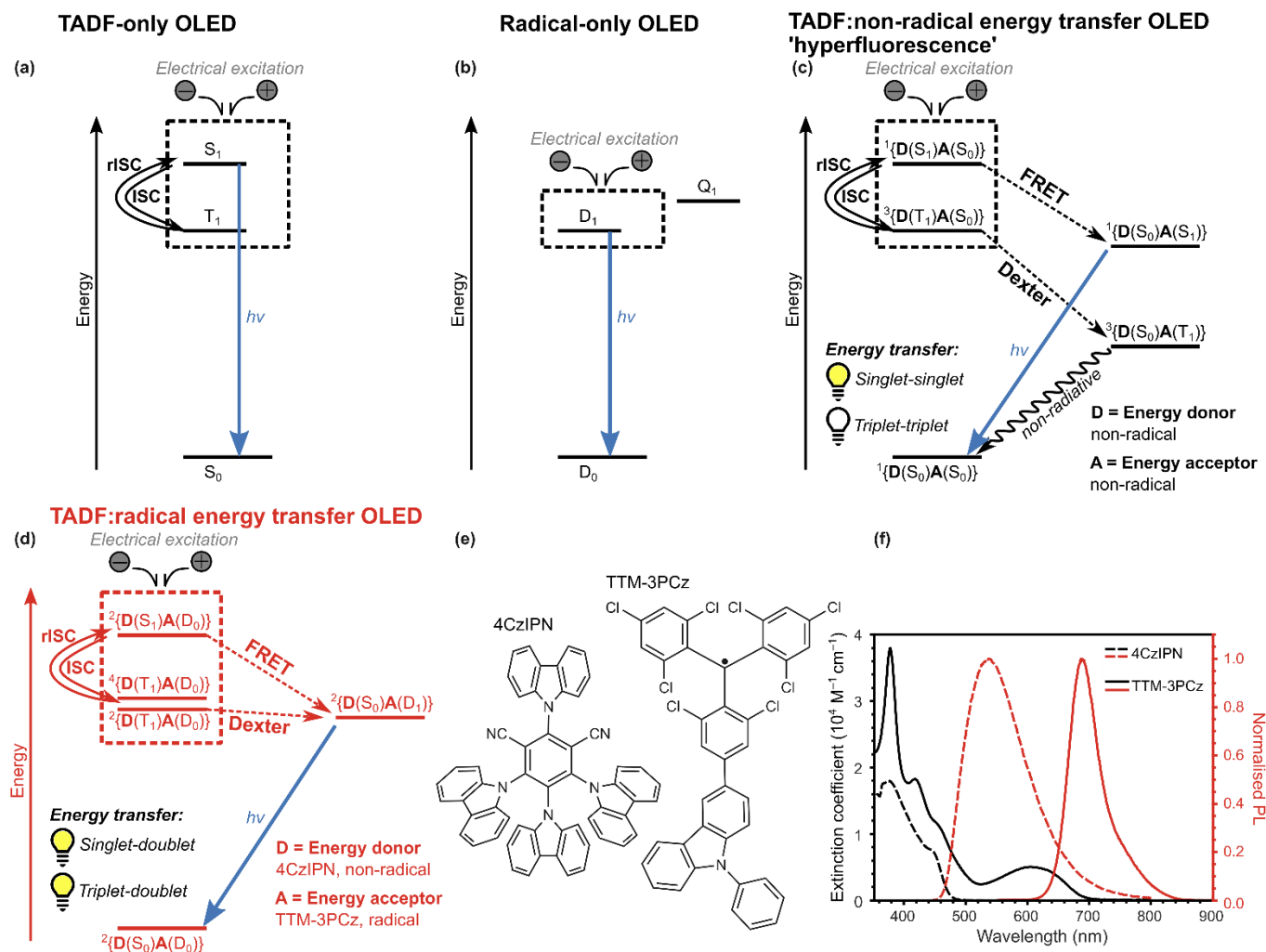


Figure 1. Light emission mechanisms and the radical energy transfer system. Electroluminescence mechanisms for TADF-only, radical-only and energy transfer OLEDs. Spin-allowed radiative transitions from excited to ground states are indicated by blue arrows labelled ' $h\nu$.' a) Scheme for TADF OLED mechanism with emission from singlet S_1 exciton, and singlet-triplet intersystem crossing (ISC) and reverse intersystem crossing (rISC) processes with non-emissive triplet T_1 exciton. b) Scheme for radical OLED mechanism with emission from doublet D_1 exciton, formed by direct electrical excitation. Higher energy and non-emissive quartet Q_1 exciton state is shown. c) Scheme for TADF:non-radical energy transfer OLED mechanism. Electrical-excitation generates singlet $D(S_1)$ and triplet $D(T_1)$ excitons, with FRET singlet-singlet energy transfer to non-radical energy acceptor (A) to form emissive singlet excitons, $A(S_1)$. Dexter triplet-triplet energy transfer forms non-emissive triplet excitons, $A(T_1)$; non-radiative decay to ground state is shown by a wavy arrow. ISC and rISC steps between $D(T_1)$ and $D(S_1)$ are indicated. Spin multiplicity of D and A pairs are denoted by $2S+1$ in $^{2S+1}\{DA\}$. d) Scheme for TADF:radical energy transfer OLED mechanism. Electrical-excitation generates singlet $D(S_1)$ and triplet $D(T_1)$ excitons, with singlet-doublet FRET and triplet-doublet Dexter energy transfer to radical energy acceptor (A) to form emissive doublet excitons, $A(D_1)$. Energy transfer mechanisms leading to dark and bright states for light emission are highlighted by dark and bright light bulbs in c) and d). e) Chemical structures for 4CzIPN and TTM-3PCz used to test the mechanism in d). f) Absorption (black) and normalised PL (red) profiles for 4CzIPN (dotted lines) and TTM-3PCz (solid lines).

As energy donors and acceptors, 4CzIPN ($E(\mathbf{D}, \text{HOMO}) = -5.8 \text{ eV}$; $E(\mathbf{D}, \text{LUMO}) = -3.4 \text{ eV}$)²⁷ and TTM-3PCz ($E(\mathbf{A}, \text{HOMO}) = -5.8\text{--}6 \text{ eV}$; $E(\mathbf{A}, \text{SOMO reduction}) = -3.7 \text{ eV}$)²⁰ were chosen, and their molecular structures are given in Fig. 1e. Singlet-doublet transfer (Fig. 1d, dotted arrow) by a dipolar fluorescence resonance energy transfer, FRET, mechanism results in conservation of doublet-spin multiplicity from $^2\{\mathbf{D}(\text{S}_1)\mathbf{A}(\text{D}_0)\}$ to $^2\{\mathbf{D}(\text{S}_0)\mathbf{A}(\text{D}_1)\}$. This was promoted by spectral overlap of TTM-3PCz \mathbf{A} -absorption and \mathbf{D} -fluorescence of 4CzIPN (Fig. 1f), a well-studied TADF emitter with a singlet-triplet exchange energy gap of $<50 \text{ meV}$.^{28,29} The small singlet-triplet energy gap also allows substantial spectral overlap of \mathbf{D} -phosphorescence and \mathbf{A} -absorption, which also leads to a resonant energy condition. This sets up conditions for triplet-doublet energy transfer by electron-exchange Dexter mechanism (Fig. 1d, dotted arrow) from long-lived ($>\text{microsecond}$) 4CzIPN triplet excitons, which can be harvested for light emission. The reverse process – doublet to triplet energy transfer – was previously demonstrated by us and others with TTM-carbazole and anthracene derivatives.³⁰ Triplet-doublet energy transfer to form $^2\{\mathbf{D}(\text{S}_0)\mathbf{A}(\text{D}_1)\}$ is spin-allowed by the $^2\{\mathbf{D}(\text{T}_1)\mathbf{A}(\text{D}_0)\}$ state, which is mixed with the $^4\{\mathbf{D}(\text{T}_1)\mathbf{A}(\text{D}_0)\}$ state because of the negligible doublet-quartet $^{2,4}\{\mathbf{D}(\text{T}_1)\mathbf{A}(\text{D}_0)\}$ energy difference (estimated to be $\sim 10 \text{ } \mu\text{eV}$ from intermolecular approach with no bond formation where antiferromagnetic coupled doublet is the lowest energy state³¹, meaning they are effectively degenerate) and spin mixing terms such as the triplet zero-field splitting interaction³². The mixed $^{2,4}\{\mathbf{D}(\text{T}_1)\mathbf{A}(\text{D}_0)\}$ states allow unlocked triplet-doublet channels for direct energy transfer with organic radicals. The theoretical considerations for singlet-doublet and triplet-doublet energy transfer by FRET and Dexter mechanisms are discussed further in SI 1.

Energy transfer photophysics with radical emitters

In order to understand the photophysics of combined TADF:radical materials we firstly studied films that were radical-only, TADF-only and TADF:radical blends. We used time-resolved optical spectroscopy measurements to probe energy transfer from 4CzIPN to TTM-3PCz on pico- to micro-second timescales. The film composition for studying the radical energy transfer concept was 4CzIPN:TTM-3PCz:CBP (ratio = 0.25:0.03:0.72). Reference films were studied for TTM-3PCz radical only (TTM-3PCz:CBP, 0.03:0.97) and 4CzIPN TADF only (4CzIPN:CBP, 0.25:0.75). The composition is based on the starting point of our previous work on TTM-3PCz OLEDs²⁰, which here allows us to test energy transfer mechanisms in proof-of-principle studies. 4CzIPN and TTM-3PCz were blended in CBP (4,4'-bis(N-carbazolyl)-1,1'-biphenyl) to reduce the effects of exciton self-

quenching³³, and with higher doping of 4CzIPN than the radical to promote charge trapping at the TADF sites and subsequent energy transfer to TTM-3PCz for light emission.

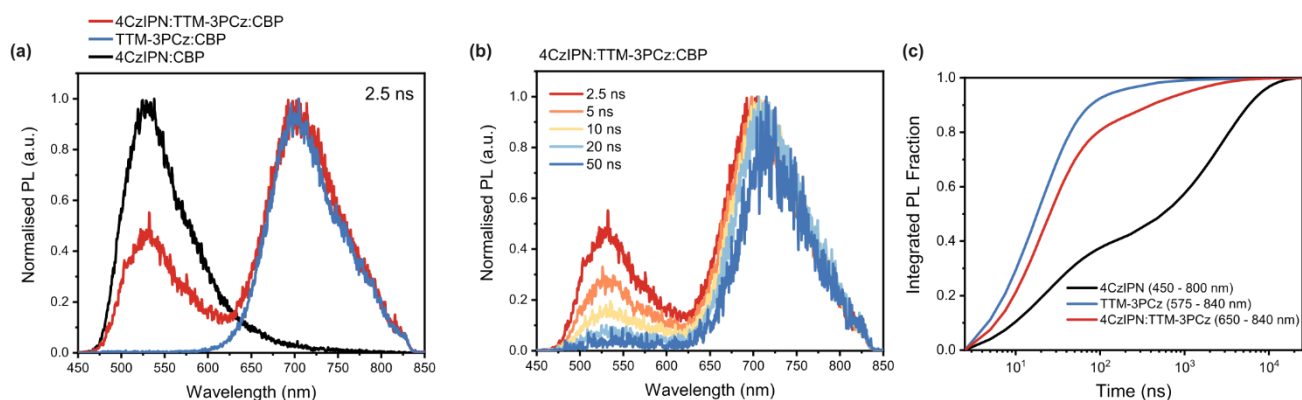


Figure 2. Transient photoluminescence studies of 4CzIPN and TTM-3PCz with 355 nm excitation. a) PL timeslices at 2.5 ns for 4CzIPN:TTM-3PCz:CBP (ratio = 0.25:0.03:0.72, red line); 4CzIPN:CBP (0.25:0.75, black line); TTM-3PCz:CBP (0.03:0.97, blue line), showing emission from both TADF and radical in the combined film. b) PL timeslices for 4CzIPN:TTM-3PCz:CBP at various times from 2.5 to 50 ns, shows the 4CzIPN emission decaying relative to the radical emission at longer times. c) Integrated PL fraction time profiles from 2.5 ns to 25 μ s for 4CzIPN:TTM-3PCz:CBP in 650-840 nm range (red line); 4CzIPN:CBP in 450-800 nm range (black line); and TTM-3PCz:CBP in 575-840 nm range (blue line), showing faster luminescence for the combined TADF:radical film than the TADF-only film.

TrPL profiles for nano-to-micro-second time ranges (with 355 nm excitation, all fluences = 5 μ J/cm²) of 4CzIPN:TTM-3PCz:CBP films are found to be superpositions of TTM-3PCz (~700 nm) and 4CzIPN (~530 nm) emission. PL timeslices (2.5 ns) are given in Fig. 2a for 4CzIPN:TTM-3PCz:CBP (red), 4CzIPN:CBP (black) and TTM-3PCz:CBP (blue). In Fig. 2b normalised PL spectra with respect to radical emission (timeslices from 2.5 to 50 ns) show substantial quenching of 4CzIPN on nanosecond timescales. For OLED applications it is desirable to reduce the overall emission time to minimise exciton quenching mechanisms,³⁴ leading us to consider plots of the integrated PL fraction for total emission (Fig. 2c). From this we observe in 4CzIPN:TTM-3PCz:CBP that 95% of all photons are emitted by 1 μ s, and over 80% of emission occurring by 100 ns. This compares favourably to 4CzIPN:CBP where only ~50% of emission happens by 1 μ s, such that the donor-acceptor blend shows faster emission than the 4CzIPN-only blend.

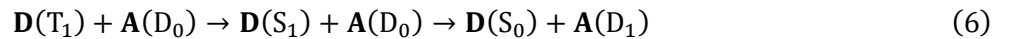
We have performed TA studies of 4CzIPN:TTM-3PCz:CBP, TTM-3PCz:CBP and 4CzIPN:CBP films in order to elucidate the energy transfer processes from excited-state absorption kinetics. In Fig. 3a $\Delta T/T$ spectral timeslices are presented for short-time TA of 4CzIPN:TTM-3PCz:CBP from 0.2-0.3 ps to 1000-1700 ps. Excitation at 400 nm allowed for the preferential formation of excitons on 4CzIPN, owing to its strong absorption

in this region and significantly higher loading fraction. The initial TA spectrum of 4CzIPN:TTM-3PCz:CBP (0.2-0.3 ps) closely resembles that of 4CzIPN:CBP, where we have assigned the 4CzIPN ground state bleach between 360-460 nm, the 4CzIPN stimulated emission overlaid on a photoinduced absorption (PIA) between 480-700 nm, and the primary 4CzIPN S_1 PIA at 830 nm (see Figs. S1 and S2 for TA of 4CzIPN:CBP films). By 10 ps we observe new PIA bands that grow in for 4CzIPN:TTM-3PCz:CBP at 620 nm, 950 nm, and 1650 nm. These features match with the TTM-3PCz D_1 spectral profile obtained from studies of TTM-3PCz:CBP films (Figs. S3 and S4), showing energy transfer from TADF singlet to radical doublet. In Fig. 3b the normalised $\Delta T/T$ kinetic profiles for 4CzIPN:TTM-3PCz:CBP in TTM-3PCz D_1 (610-630 nm, red line) and 4CzIPN S_1 (800-830 nm, orange line) PIA regions are shown. We highlight an additional quenching of 4CzIPN in 4CzIPN:TTM-3PCz:CBP compared to 4CzIPN:CBP films (black line, Fig. 3b). The quenching of 4CzIPN S_1 PIA and the growth of TTM-3PCz D_1 PIA on picosecond timescales prior to nanosecond 4CzIPN intersystem crossing is attributed to Förster-type singlet-doublet energy transfer.³⁵ As the 4CzIPN S_1 PIA lies in a region where there is reduced absorption by the TTM-3PCz D_1 , we can use the $\Delta T/T$ with and without the presence of TTM-3PCz to estimate a lower bound for the fraction of singlet-doublet energy transfer. By 1.7 ns, the 4CzIPN S_1 PIA falls to approximately 45% and 60% of the initial signal with (orange) and without (black) TTM-3PCz present, respectively, suggesting that $\geq 15\%$ of S_1 from 4CzIPN have already undergone fluorescence resonance energy transfer (FRET) to TTM-3PCz in 4CzIPN:TTM-3PCz:CBP. With selective excitation of TTM-3PCz at 600 nm (below the 4CzIPN bandgap) in 4CzIPN:TTM-3PCz:CBP, the resulting TA profiles resemble TTM-3PCz:CBP, showing that the D_1 exciton – once formed – does not interact with 4CzIPN by further energy or charge transfer processes (Figs. S5 and S6).

We have studied energy transfer for timescales beyond 1 ns with long-time TA measurements of 4CzIPN:TTM-3PCz:CBP films (excited at 355 nm). $\Delta T/T$ spectral timeslices (1-2 ns to 1000-2000 ns) in Fig. 3c display features at 620 nm, 830 nm and 1600 nm, which can be attributed to the TTM-3PCz D_1 PIA and 4CzIPN S_1 PIA from radical-only (Figs. S3 and S4) and TADF-only films (Figs. S5 and S6). The kinetic decay profile of the TTM-3PCz PIA (600-630 nm) has an extended lifetime in 4CzIPN:TTM-3PCz:CBP films (red squares, Fig. 3d) compared to TTM-3PCz:CBP (black circles). The 4CzIPN:TTM-3PCz:CBP kinetic profile can be fitted to a bi-exponential with time constants of $\tau_1 = 18.8$ ns and $\tau_2 = 1.6$ μ s. The presence of a long-lived D_1 state in 4CzIPN:TTM-3PCz:CBP, beyond the D_1 excited-state lifetime measured from TTM-3PCz:CBP ($\tau = 16.8$ ns,

Fig. S4), suggests energy transfer from 4CzIPN triplet (T_1) states. By comparing the kinetic traces of the PIA associated with 4CzIPN from 800-830 nm in 4CzIPN:CBP (black circles, Fig. 3e) and 4CzIPN:TTM-3PCz:CBP (red squares), we observed reductions in both the prompt and delayed lifetimes, from 12.1 ns to 7.8 ns and 2.5 μ s to 1.0 μ s, respectively, from the presence of TTM-3PCz. This provides further evidence for energy transfer from 4CzIPN T_1 (delayed kinetic), and additionally from 4CzIPN S_1 (prompt kinetic), to form TTM-3PCz D_1 .

Triplet-doublet energy transfer from 4CzIPN, a TADF molecule, can be attributed to a hyperfluorescent-type mechanism by breakout from S_1 - T_1 ISC and rISC cycles,³⁶



i.e. 4CzIPN reverse intersystem crossing, then singlet-doublet Förster transfer, or triplet-doublet direct Dexter-type mechanism^{37,38} as given in Eq. (4). Both mechanisms lead to reduced T_1 lifetime. In order to distinguish the energy transfer mechanisms we have performed temperature dependence studies (50-293 K) on trPL of 4CzIPN:CBP (Fig. S10) and 4CzIPN:TTM-3PCz:CBP (Fig. S11). In both films there is negligible temperature dependence on trPL up to 100 ns, which we define as the prompt emission; we classify light emission from 100 ns onwards as delayed type. The ratio of integrated delayed emission at different temperatures (T) with respect to the integrated value at 293 K is shown in Fig. 4f (i.e. Delayed PL(T)/Delayed PL($T = 293$ K)). The delayed PL ratio is reduced in 4CzIPN:CBP films compared to 4CzIPN:TTM-3PCz:CBP, falling to 0.2 and 0.8 at 50 K, respectively. This supports a Dexter-type triplet-doublet energy transfer channel in 4CzIPN:TTM-3PCz:CBP, with lower activation energy than reverse intersystem in 4CzIPN:CBP for thermally activated delayed fluorescence. However, the signal:noise for delayed PL ratio varies in 4CzIPN:TTM-3PCz:CBP with changing temperature, restricting further quantitative analysis.

From the film photophysical studies we have demonstrated efficient singlet-doublet and triplet-doublet energy transfer in 4CzIPN:TTM-3PCz:CBP from picosecond to microsecond timescales, which we have attributed to Förster and Dexter mechanisms that enable luminescent TADF:radical films with emission from radical D_1 .

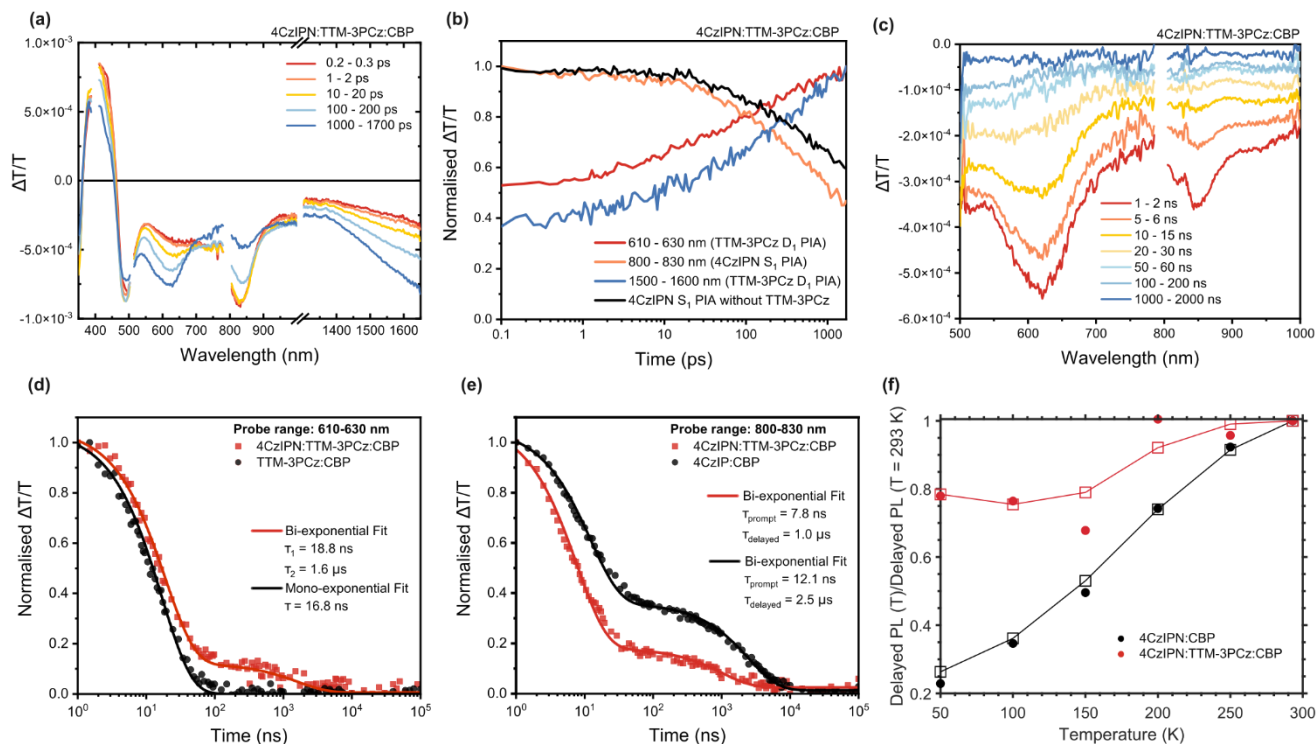


Figure 3. Transient absorption and temperature dependence studies of 4CzIPN and TTM-3PCz. Picosecond to nanosecond a) timeslices and b) kinetic profiles from transient absorption studies of 4CzIPN:TTM-3PCz:CBP (ratio = 0.25:0.03:0.72). 400 nm excitation, fluence = 89.1 $\mu\text{J}/\text{cm}^2$. This shows decay of the singlet PIA around 830nm and the growth of the radical PIAs around 620 and 1650 nm. c) Nanosecond to microsecond timeslices of the 4CzIPN:TTM-3PCz:CBP blend (0.25:0.03:0.72). 355 nm excitation, fluence = 17.0 $\mu\text{J}/\text{cm}^2$. Transient absorption kinetic profiles for photoinduced absorption features of d) TTM-3PCz (610-630 nm) and e) 4CzIPN (800-830 nm). In d) TTM-3PCz excited-state kinetics are shown for 4CzIPN:TTM-3PCz:CBP (0.25:0.03:0.72, red squares); and TTM-3PCz:CBP (0.03:0.97, black circles). This shows delayed radical emission is active in 4CzIPN:TTM-3PCz:CBP (TADF:radical) from triplet-doublet energy transfer. In e) 4CzIPN excited-state kinetics are shown for 4CzIPN:TTM-3PCz:CBP (red squares); and 4CzIPN:CBP (0.25:0.75, black circles). This shows delayed radical emission in 4CzIPN:TTM-3PCz:CBP (TADF:radical) is more rapid than delayed emission in 4CzIPN:CBP (TADF-only). Mono- and bi-exponential fits are indicated by solid lines in d) and e). f) Ratio of integrated delayed PL contribution for 4CzIPN:CBP (black circles) and 4CzIPN:TTM-3PCz:CBP (red circles) at different temperatures. 3-point moving average and trends for these profiles are indicated by square and line plots, and show different temperature dependencies.

Radical OLEDs and magneto-electroluminescence studies

Following our demonstration of singlet-triplet-doublet energy transfer photophysics, we aimed to exploit these processes in more efficient radical-based OLED designs. We fabricated TADF:radical OLEDs using the device structure in Fig. 4a. B3PYMPM (4,6-bis(3,5-di(pyridine-3-yl)phenyl)-2-methylpyrimidine) and TAPC (1,1-bis[(di-4-tolylamino)phenyl]cyclohexane) were used as electron transport and hole transport layers, respectively.

The emissive layer (EML) was 4CzIPN:TTM-3PCz:CBP (0.25:0.03:0.72) – the same composition as the photophysics studies. Single-dopant OLEDs were also fabricated where EML was 4CzIPN:CBP (0.25:0.75) for TADF reference devices; and EML was TTM-3PCz:CBP (0.03:0.97) for radical reference OLEDs.

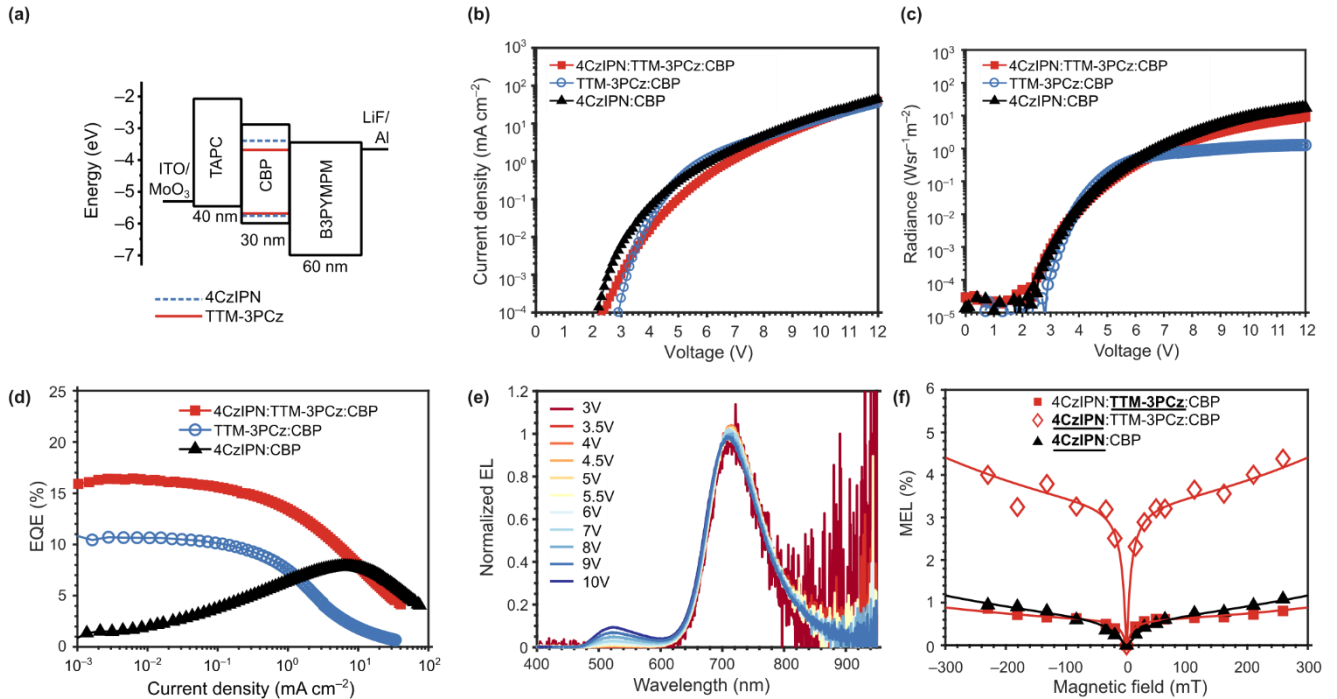


Figure 4. 4CzIPN and TTM-3PCz organic light-emitting diodes. a) Device architecture for OLEDs with varying emissive layer: 4CzIPN:TTM-3PCz:CBP, 4CzIPN:CBP; TTM-3PCz:CBP. b-d) Current density-voltage (J-V), radiance-voltage, EQE-current density (from 10^{-3} mA/cm²) curves for OLEDs. e) Normalised EL profiles for 4CzIPN:TTM-3PCz:CBP OLEDs with varying voltage, and 4CzIPN and TTM-3PCz emission contributions. f) Magneto-electroluminescence (MEL) studies of TTM-3PCz (red squares) and 4CzIPN (red diamonds) emission in 4CzIPN:TTM-3PCz:CBP OLEDs; 4CzIPN emission in 4CzIPN:CBP (black triangles). OLED devices were biased at 8V. MEL studies show different magnetic field dependencies for 4CzIPN and TTM-3PCz emission from 4CzIPN:TTM-3PCz:CBP devices, which supports Dexter triplet-doublet energy transfer and not the hyperfluorescence mechanism of 4CzIPN triplet exciton energy harvesting.

The current density-voltage (J-V), radiance-voltage and EQE plots for the 4CzIPN:TTM-3PCz:CBP (red squares), 4CzIPN:CBP (black triangles) and TTM-3PCz:CBP (blue circles) OLEDs are shown in Fig. 4b-d. We found that the turn-on voltages decrease from 2.9 V (TTM-3PCz:CBP device) to 2.3 V (4CzIPN:TTM-3PCz:CBP) to 2.2 V (4CzIPN:CBP). Here we define the turn-on voltage to be that corresponding to current density >0.1 μ A/cm², above the electrical noise level of the devices. The trend in turn-on voltage suggests that the inclusion of the TADF sensitizer leverages more energy efficient doublet exciton formation in electroluminescence. However, the higher turn-on voltage for TADF:radical OLEDs compared to TADF, and different J-V profiles in

Fig. 3b, imply that both CBP and 4CzIPN mediate some electrical excitation of TTM-3PCz in TADF:radical devices. If all doublet electroluminescence originated by energy transfer from TADF sensitisation as in Fig. 1d, the J-V curves and turn-on voltages would be identical for 4CzIPN:CBP and 4CzIPN:TTM-3PCz:CBP OLEDs.

We note there is a plateau in maximum radiance of $\sim 1 \text{ W sr}^{-1} \text{ m}^{-2}$ from 5 V for TTM-3PCz:CBP devices in Fig. 4c; radiance values up to $10 \text{ W sr}^{-1} \text{ m}^{-2}$ are achievable in 4CzIPN:TTM-3PCz:CBP. At voltages higher than 5 V, there is increasing component of 4CzIPN emission in the total EL of 4CzIPN:TTM-3PCz:CBP OLEDs. At 10 V the EL from the device contains 89% TTM-3PCz and 11% 4CzIPN contributions. The higher radiance at 10 V for 4CzIPN:TTM-3PCz:CBP ($5.0 \text{ W sr}^{-1} \text{ cm}^{-2}$) compared to TTM-3PCz:CBP ($1.1 \text{ W sr}^{-1} \text{ cm}^{-2}$) in Fig. 4c is therefore consistent with increasing energy transfer contribution from electrically excited 4CzIPN. The EL profile at 10 V in Fig. 4e resembles the steady-state PL profile for 4CzIPN:TTM-3PCz blends (Fig. S8).

Fig. 4d shows that there is substantial increase in maximum EQE on going from 4CzIPN:CBP (7.8 %) and TTM-3PCz:CBP (10.7 %) devices to 4CzIPN:TTM-3PCz:CBP (16.4 %) OLEDs. The EQE is evaluated for the total EL output. J_0 , the critical current density that corresponds to the device current at half the maximum EQE, increases from 2.1 mA cm^{-2} for TTM-3PCz:CBP to 9.5 mA cm^{-2} for 4CzIPN:TTM-3PCz:CBP. The better roll-off and sustained EL efficiency in 4CzIPN:TTM-3PCz:CBP OLEDs is attributed to an increasing contribution of 4CzIPN energy transfer to the EL at higher current densities. At lower voltages ($< 5 \text{ V}$) and current densities ($< 0.1 \text{ mA cm}^{-2}$), the EL shows TTM-3PCz emission only (Fig. 4e). We performed studies to obtain the device half-lifetime, T50 (time for luminance to fall to half of the initial value under a constant current density). The T50 of energy transfer-type 4CzIPN:TTM-3PCz:CBP OLEDs was found to be 42 min at 0.4 mA/cm^2 (see Fig. S7), indicating some improvement over charge-trapping-type devices that we have previously reported for radical OLEDs with TTM-derivative:host EML (10 min at 0.1 mA/cm^2).²⁵

Magneto-electroluminescence (MEL) and magneto-conductance (MC) studies have been performed on the 4CzIPN:CBP and 4CzIPN:TTM-3PCz:CBP devices. The devices were biased at 8 V and the data for magneto-EL and magneto-conductance were collected simultaneously. In 4CzIPN:CBP devices, MEL and MC profiles show enhanced EL and current density upon application of magnetic field (Fig. 4f, Fig. S9). The profiles are fitted to double Lorentzian functions that capture low ($< 10 \text{ mT}$) and high ($> 10 \text{ mT}$) magnetic field effects (MFEs). The low field dependence is characteristic of magnetic field effects on hyperfine-mediate spin mixing of singlet and triplet polaron pair,³⁹ the precursors of excitons, which affect the ratio of singlet and triplet exciton formation.

High field effects can arise from triplet exciton-polaron quenching and singlet-triplet dephasing effects.^{40,41} MFEs of 4CzIPN:CBP devices are positive and show typical behaviour for MEL and MC from non-radical dopant systems, as previously reported.⁴²

In TADF:radical OLEDs (4CzIPN:TTM-3PCz:CBP) we have studied magnetic field effects on EL from TTM-3PCz (680–800 nm) and 4CzIPN (500–550 nm) emission contributions. We observe positive magnetic field effects for both TTM-3PCz and 4CzIPN contributions, which indicates that the main magnetic field sensitivity originates from hyperfine-mediated spin mixing of singlet-triplet polaron pairs, as found in the TADF only devices. However the size of MEL for 4CzIPN (+4% at 250 mT) and TTM-3PCz (+1% at 250 mT) emission components are different in TADF:radical OLEDs. We consider that non-identical MEL profiles for 4CzIPN and TTM-3PCz emission in 4CzIPN:TTM-3PCz:CBP devices supports a Dexter triplet-doublet energy transfer mechanism, because an identical field sensitivity would be expected for the 4CzIPN and TTM-3PCz MEL in TADF:radical hyperfluorescent-type devices.

Conclusions

We have demonstrated efficient energy transfer of 4CzIPN singlet and triplet excitons to obtain emissive doublet excitons of TTM-3PCz. In trPL studies we observed more rapid light emission in 4CzIPN:TTM-3PCz:CBP blends than 4CzIPN:CBP, as up to 95% and 50% of photons are emitted by 1 μ s, respectively. TA measurements revealed singlet-doublet and triplet-doublet energy transfer on 10-100 ns and 100 ns–1 μ s timescales, though the observed timescale of triplet transfer is limited by the time taken for intersystem crossing to take place on 4CzIPN and, as a spin-allowed process, may be faster than this. OLEDs with 4CzIPN:TTM-3PCz:CBP emissive layer were demonstrated with max EQE = 16.4% and $J_0 = 9.5 \text{ mA/cm}^2$, which outperforms TTM-3PCz:CBP (max EQE = 10.7%, $J_0 = 2.1 \text{ mA/cm}^2$) for the same charge transport layer architecture. With also an order of magnitude improvement in device stability, the energy transfer-type radical OLEDs therefore show a substantial improvement in device characteristics compared to previous reports of charge-trapping radical OLEDs. The MEL results allow us to rule out a fully hyperfluorescence-type (Eq. 6) mechanism for EL, and support Dexter-type T_1 - D_1 energy transfer pathways enabled by organic radicals, here TTM-3PCz. We highlight that Dexter triplet-triplet transfer from energy donor to acceptor is a loss route for light emission with non-radicals, and must be suppressed in energy transfer devices using non-radical fluorescent emitters, for example, hyperfluorescence-

type devices.¹⁵ However fluorescent radical (doublet) emitters can exploit the triplet-doublet energy transfer pathway for radical OLEDs as we have demonstrated here, without a lower-lying radical ‘triplet state’ that must be avoided for emission losses. By unlocking new energy transfer channels, an optoelectronic design for improved radical-based light-emitting devices is enabled by their unpaired electron spin properties.

Acknowledgements

JD, ZC and FL are grateful for financial support from the National Natural Science Foundation of China (grant no. 51925303) and the programme ‘JLUSTIRT’ (grant no. 2019TD-33). EWE is grateful to the Leverhulme Trust for an Early Career Fellowship; and Royal Society for a University Research Fellowship (grant no. URF\R1\201300). TJHH thanks the Royal Society for a University Research Fellowship (grant no. URF\R1\201502). FL is an academic visitor at the Cavendish Laboratory, Cambridge, and is supported by the Talents Cultivation Programme (Jilin University, China). AJG and RHF acknowledge support from the Simons Foundation (grant no. 601946) and the EPSRC (EP/M01083X/1 and EP/M005143/1). This project has received funding from the ERC under the European Union’s Horizon 2020 research and innovation programme (grant agreement no. 670405).

Author Contributions

EWE and FL fabricated thin-films and OLED devices, which were characterised by photoluminescence, J-V-radiance measurements and magnetic field studies. AJG performed transient absorption measurements. AJG and EWE carried out the transient PL measurements. QG conducted OLED time dependence studies. JD and ZC synthesised the radical materials. TJHH formulated theory on the photophysical mechanisms. EWE, RHF and FL conceived the project and supervised the work. The results were analysed and the manuscript was written with input from all authors.

Additional information

Supplementary information accompanies this paper at [to be completed in proofs]

Competing financial interests

The authors declare no competing interests.

Methods

Materials

TTM-3PCz was synthesised as previously reported²⁰. 4CzIPN, TAPC, B3PYMPM, CBP of sublimed grade and other OLED materials were obtained from Ossila, Xi'an Polymer Light and Lumtec.

Photophysics

TrPL and TA studies were performed on home-built setups powered by a Ti:sapphire amplifier (Spectra Physics Solstice Ace, 100 fs pulses at 800 nm, 7 W output at 1 kHz). TrPL profiles were recorded using an Andor spectrometer setup with electrically gated intensified CCD camera (Andor SR303i; Andor iStar). Sample excitation with 400 nm pump pulse was provided by frequency-doubled 800 nm pulse from Ti:sapphire amplifier in trPL and short-time (ps–ns) TA studies. Short-time TA studies with 600 nm excitation were achieved from the wavelength tuneable output of TOPAS optical parametric amplifier (Light Conversion), which was pumped by the 800 nm laser pulses from the Ti:sapphire amplifier. Long-time (ns– μ s) TA studies were performed with 355 nm pump pulses from an Innolas Piccolo 25. Probe pulses for TA were obtained from non-collinear optical parametric amplifier (NOPA) systems for the visible (500–780 nm), near infrared (830–1000 nm) and infrared (1250–1650 nm) wavelength ranges. The NOPA probe pulses were divided into two identical beams by a 50/50 beamsplitter; this allowed for the use of a second reference beam for improved signal:noise. The probe pulse for the UV (350–500 nm) region was provided by a white light supercontinuum generated in a CaF₂ crystal. The probe pulses were detected by Si (Hamamatsu S8381-1024Q) and InGaAs (Hamamatsu G11608-512DA) dual-line array with a custom-built board from Stresing Entwicklungsbüro.

Device fabrication and characterisation

Organic semiconductor films and devices were fabricated by vacuum-deposition processing ($< 6 \times 10^{-7}$ torr) using an Angstrom Engineering EvoVac 700 system. Current density, voltage and electroluminescence characteristics were measured using a Keithley 2400 sourcemeter, Keithley 2000 multimeter and calibrated silicon photodiode. The EL spectra were recorded by an Ocean Optics Flame spectrometer. Magneto-EL measurements were performed with Andor spectrometer (Shamrock 303i and iDus camera) for modulation of EL in presence of magnetic field applied by GMW 3470 electromagnet.

References

- (1) Tang, C. W.; VanSlyke, S. A. Organic Electroluminescent Diodes. *Appl. Phys. Lett.* **1987**, *51* (12), 913–915. <https://doi.org/10.1063/1.98799>.
- (2) Forrest, S. R.; O'Brien, D. F.; Baldo, M. A.; O'Brien, D. F.; Thompson, M. E.; Forrest, S. R. Excitonic Singlet-Triplet Ratio in a Semiconducting Organic Thin Film. **1999**, *60* (20), 14422–14428. <https://doi.org/10.1103/PhysRevB.60.14422>.
- (3) Kido, J.; Iizumi, Y. Fabrication of Highly Efficient Organic Electroluminescent Devices. *Appl. Phys. Lett.* **1998**, *73* (19), 2721–2723. <https://doi.org/10.1063/1.122570>.
- (4) Di, D.; Yang, L.; Richter, J. M.; Meraldi, L.; Altamimi, R. M.; Alyamani, A. Y.; Credgington, D.; Musselman, K. P.; MacManus-Driscoll, J. L.; Friend, R. H. Efficient Triplet Exciton Fusion

in Molecularly Doped Polymer Light-Emitting Diodes. *Adv. Mater.* **2017**, *29* (13).
<https://doi.org/10.1002/adma.201605987>.

- (5) Baldo, M. A.; O'Brien, D. F.; You, Y.; Shoustikov, A.; Sibley, S.; Thompson, M. E.; Forrest, S. R. Highly Efficient Phosphorescent Emission from Organic Electroluminescent Devices. *Nature* **1998**, *395* (6698), 151–154. <https://doi.org/10.1038/25954>.
- (6) Ma, Y.; Houyu, Z.; Shen, J.; Che, C. Electroluminescence from Triplet Metal-Ligand Charge-Transfer Excited State of Transition Metal Complexes. *Synth. Met.* **1998**, *94* (3), 245–248. [https://doi.org/10.1016/s0379-6779\(97\)04166-0](https://doi.org/10.1016/s0379-6779(97)04166-0).
- (7) Adachi, C.; Baldo, M. A.; Thompson, M. E.; Forrest, S. R. Nearly 100% Internal Phosphorescence Efficiency in an Organic Light-Emitting Device. *J. Appl. Phys.* **2001**, *90* (10), 5048–5051. <https://doi.org/10.1063/1.1409582>.
- (8) Uoyama, H.; Goushi, K.; Shizu, K.; Nomura, H.; Adachi, C. Highly Efficient Organic Light-Emitting Diodes from Delayed Fluorescence. *Nature* **2012**, *492* (7428), 234–240. <https://doi.org/10.1038/nature11687>.
- (9) Shizu, K.; Uejima, M.; Nomura, H.; Sato, T.; Tanaka, K.; Kaji, H.; Adachi, C. Enhanced Electroluminescence from a Thermally Activated Delayed-Fluorescence Emitter by Suppressing Nonradiative Decay. *Phys. Rev. Appl.* **2015**, *3* (1), 014001. <https://doi.org/10.1103/PhysRevApplied.3.014001>.
- (10) Kim, D. H.; D'Aléo, A.; Chen, X. K.; Sandanayaka, A. D. S.; Yao, D.; Zhao, L.; Komino, T.; Zaborova, E.; Canard, G.; Tsuchiya, Y.; Choi, E.; Wu, J. W.; Fages, F.; Brédas, J. L.; Ribierre, J. C.; Adachi, C. High-Efficiency Electroluminescence and Amplified Spontaneous Emission from a Thermally Activated Delayed Fluorescent Near-Infrared Emitter. *Nat. Photonics* **2018**, *12* (2), 98–104. <https://doi.org/10.1038/s41566-017-0087-y>.
- (11) Kotadiya, N. B.; Blom, P. W. M.; Wetzelaer, G. J. A. H. Efficient and Stable Single-Layer Organic Light-Emitting Diodes Based on Thermally Activated Delayed Fluorescence. *Nat. Photonics* **2019**, *13* (11), 765–769. <https://doi.org/10.1038/s41566-019-0488-1>.
- (12) Hu, Y.; Cai, W.; Ying, L.; Chen, D.; Yang, X.; Jiang, X. F.; Su, S.; Huang, F.; Cao, Y. Novel Efficient Blue and Bluish-Green Light-Emitting Polymers with Delayed Fluorescence. *J. Mater. Chem. C* **2018**, *6* (11), 2690–2695. <https://doi.org/10.1039/c7tc04064d>.
- (13) Nakanotani, H.; Higuchi, T.; Furukawa, T.; Masui, K.; Morimoto, K.; Numata, M.; Tanaka, H.; Sagara, Y.; Yasuda, T.; Adachi, C. High-Efficiency Organic Light-Emitting Diodes with Fluorescent Emitters. *Nat. Commun.* **2014**, *5* (May), 1–7. <https://doi.org/10.1038/ncomms5016>.
- (14) Chan, C. Y.; Tanaka, M.; Lee, Y. T.; Wong, Y. W.; Nakanotani, H.; Hatakeyama, T.; Adachi, C. Stable Pure-Blue Hyperfluorescence Organic Light-Emitting Diodes with High-Efficiency and Narrow Emission. *Nat. Photonics* **2021**, *15* (3), 203–207. <https://doi.org/10.1038/s41566-020-00745-z>.
- (15) Abroshan, H.; Coropceanu, V.; Brédas, J. L. Hyperfluorescence-Based Emission in Purely Organic Materials: Suppression of Energy-Loss Mechanisms via Alignment of Triplet Excited States. *ACS Mater. Lett.* **2020**, *2* (11), 1412–1418. <https://doi.org/10.1021/acsmaterialslett.0c00407>.
- (16) Cui, L. S.; Gillett, A. J.; Zhang, S. F.; Ye, H.; Liu, Y.; Chen, X. K.; Lin, Z. Sen; Evans, E. W.; Myers, W. K.; Ronson, T. K.; Nakanotani, H.; Reineke, S.; Bredas, J. L.; Adachi, C.; Friend, R.

- H. Fast Spin-Flip Enables Efficient and Stable Organic Electroluminescence from Charge-Transfer States. *Nat. Photonics* **2020**, *14* (10), 636–642. <https://doi.org/10.1038/s41566-020-0668-z>.
- (17) Zhang, D.; Duan, L.; Li, C.; Li, Y.; Li, H.; Zhang, D.; Qiu, Y. High-Efficiency Fluorescent Organic Light-Emitting Devices Using Sensitizing Hosts with a Small Singlet-Triplet Exchange Energy. *Adv. Mater.* **2014**, *26* (29), 5050–5055. <https://doi.org/10.1002/adma.201401476>.
- (18) Peng, Q.; Obolda, A.; Zhang, M.; Li, F. Organic Light-Emitting Diodes Using a Neutral π Radical as Emitter: The Emission from a Doublet. *Angew. Chemie - Int. Ed.* **2015**, *54* (24), 7091–7095. <https://doi.org/10.1002/anie.201500242>.
- (19) Neier, E.; Arias Ugarte, R.; Rady, N.; Venkatesan, S.; Hudnall, T. W.; Zakhidov, A. Solution-Processed Organic Light-Emitting Diodes with Emission from a Doublet Exciton; Using (2,4,6-Trichlorophenyl)methyl as Emitter. *Org. Electron.* **2017**, *44*, 126–131. <https://doi.org/10.1016/j.orgel.2017.02.010>.
- (20) Ai, X.; Evans, E. W.; Dong, S.; Gillett, A. J.; Guo, H.; Chen, Y.; Hele, T. J. H.; Friend, R. H.; Li, F. Efficient Radical-Based Light-Emitting Diodes with Doublet Emission. *Nature* **2018**, *563* (7732), 536–540. <https://doi.org/10.1038/s41586-018-0695-9>.
- (21) Cui, Z.; Abdurahman, A.; Ai, X.; Li, F. Stable Luminescent Radicals and Radical-Based LEDs with Doublet Emission. *CCS Chem.* **2020**, *2* (4), 1129–1145. <https://doi.org/10.31635/ccschem.020.202000210>.
- (22) Hudson, J. M.; Hele, T. J. H.; Evans, E. W. Efficient Light-Emitting Diodes from Organic Radicals with Doublet Emission. *J. Appl. Phys.* **2021**, *129* (18), 180901. <https://doi.org/10.1063/5.0047636>.
- (23) Hattori, Y.; Michail, E.; Schmiedel, A.; Moos, M.; Holzapfel, M.; Krummenacher, I.; Braunschweig, H.; Müller, U.; Pflaum, J.; Lambert, C. Luminescent Mono-, Di-, and Triradicals: Bridging Polychlorinated Triarylmethyl Radicals by Triarylamines and Triarylboranes. *Chem. - A Eur. J.* **2019**, *25* (68), 15463–15471. <https://doi.org/10.1002/chem.201903007>.
- (24) Hattori, Y.; Kusamoto, T.; Nishihara, H. Luminescence, Stability, and Proton Response of an Open-Shell (3,5-Dichloro-4-Pyridyl)Bis(2,4,6-Trichlorophenyl)methyl Radical. *Angew. Chemie* **2014**, *126* (44), 12039–12042. <https://doi.org/10.1002/ange.201407362>.
- (25) Abdurahman, A.; Hele, T. J. H.; Gu, Q.; Zhang, J.; Peng, Q.; Zhang, M.; Friend, R. H.; Li, F.; Evans, E. W. Understanding the Luminescent Nature of Organic Radicals for Efficient Doublet Emitters and Pure-Red Light-Emitting Diodes. *Nat. Mater.* **2020**, *19* (11), 1224–1229. <https://doi.org/10.1038/s41563-020-0705-9>.
- (26) Hiratsuka, H.; Rajadurai, S.; Das, P. K.; Hug, G. L.; Fessenden, R. W. Evidence for Non-Radiative Triplet-Doublet Energy Transfer in the Naphthalene-Benzophenone System in Tetrahydrofuran. *Chem. Phys. Lett.* **1987**, *137* (3), 255–260. [https://doi.org/10.1016/0009-2614\(87\)80215-4](https://doi.org/10.1016/0009-2614(87)80215-4).
- (27) Nakanotani, H.; Masui, K.; Nishide, J.; Shibata, T.; Adachi, C. Promising Operational Stability of High-Efficiency Organic Light-Emitting Diodes Based on Thermally Activated Delayed Fluorescence. *Sci. Rep.* **2013**, *3* (1), 1–6. <https://doi.org/10.1038/srep02127>.

- (28) Niwa, A.; Kobayashi, T.; Nagase, T.; Goushi, K.; Adachi, C.; Naito, H. Temperature Dependence of Photoluminescence Properties in a Thermally Activated Delayed Fluorescence Emitter. *Appl. Phys. Lett.* **2014**, *104* (21), 213303. <https://doi.org/10.1063/1.4878397>.
- (29) Menke, S. M.; Holmes, R. J. Exciton Transport in an Organic Semiconductor Exhibiting Thermally Activated Delayed Fluorescence. *J. Phys. Chem. C* **2016**, *120* (16), 8502–8508. <https://doi.org/10.1021/acs.jpcc.6b01679>.
- (30) Han, J.; Jiang, Y.; Obolda, A.; Duan, P.; Li, F.; Liu, M. Doublet – Triplet Energy Transfer-Dominated Photon Upconversion. **2017**, 5865–5870. <https://doi.org/10.1021/acs.jpcclett.7b02677>.
- (31) Kawai, A.; Shibuya, K. Charge-Transfer Controlled Exchange Interaction in Radical-Triplet Encounter Pairs as Studied by FT-EPR Spectroscopy. *J. Phys. Chem. A* **2007**, *111* (23), 4890–4901. <https://doi.org/10.1021/jp067753d>.
- (32) Ern, V.; Merrifield, R. E. Magnetic Field Effect on Triplet Exciton Quenching in Organic Crystals. *Phys. Rev. Lett.* **1968**, *21* (9), 609–611. <https://doi.org/10.1103/PhysRevLett.21.609>.
- (33) Kim, H. S.; Park, S. R.; Suh, M. C. Concentration Quenching Behavior of Thermally Activated Delayed Fluorescence in a Solid Film. *J. Phys. Chem. C* **2017**, *121* (26), 13986–13997. <https://doi.org/10.1021/acs.jpcc.7b02369>.
- (34) Murawski, C.; Leo, K.; Gather, M. C. Efficiency Roll-Off in Organic Light-Emitting Diodes. *Adv. Mater.* **2013**, *25* (47), 6801–6827. <https://doi.org/10.1002/adma.201301603>.
- (35) Förster, T. 10th Spiers Memorial Lecture. Transfer Mechanisms of Electronic Excitation. *Discussions of the Faraday Society*. The Royal Society of Chemistry January 1, 1959, pp 7–17. <https://doi.org/10.1039/DF9592700007>.
- (36) Yurash, B.; Nakanotani, H.; Olivier, Y.; Beljonne, D.; Adachi, C.; Nguyen, T. Q. Photoluminescence Quenching Probes Spin Conversion and Exciton Dynamics in Thermally Activated Delayed Fluorescence Materials. *Adv. Mater.* **2019**, *31* (21), 1804490. <https://doi.org/10.1002/adma.201804490>.
- (37) Dexter, D. L. A Theory of Sensitized Luminescence in Solids. *J. Chem. Phys.* **1953**, *21* (5), 836–850. <https://doi.org/10.1063/1.1699044>.
- (38) Sudha Devi, L.; Al-Suti, M. K.; Dosche, C.; Khan, M. S.; Friend, R. H.; Köhler, A. Triplet Energy Transfer in Conjugated Polymers. I. Experimental Investigation of a Weakly Disordered Compound. *Phys. Rev. B - Condens. Matter Mater. Phys.* **2008**, *78* (4), 045210. <https://doi.org/10.1103/PhysRevB.78.045210>.
- (39) Nguyen, T. D.; Hukic-Markosian, G.; Wang, F.; Wojcik, L.; Li, X. G.; Ehrenfreund, E.; Vardeny, Z. V. Isotope Effect in Spin Response of π -Conjugated Polymer Films and Devices. *Nat. Mater.* **2010**, *9* (4), 345–352. <https://doi.org/10.1038/nmat2633>.
- (40) Joseph E. Lawrence, Alan M. Lewis, David E. Manolopoulos, P. J. H. Magneto-electroluminescence in Organic Light-Emitting Diodes. *J. Chem. Phys.* **2016**, *144*, 21409. <https://doi.org/10.1063/1.4953093>.
- (41) Keevers, T. L.; Baker, W. J.; McCamey, D. R. Theory of Exciton-Polaron Complexes in Pulsed Electrically Detected Magnetic Resonance. *Phys. Rev. B - Condens. Matter Mater. Phys.* **2015**, *91* (20), 205206. <https://doi.org/10.1103/PhysRevB.91.205206>.

- (42) Tanaka, M.; Nagata, R.; Nakanotani, H.; Adachi, C. Understanding Degradation of Organic Light-Emitting Diodes from Magnetic Field Effects. *Commun. Mater.* **2020**, *1* (1), 1–9. <https://doi.org/10.1038/s43246-020-0019-0>.

Supplementary Information:

Singlet and triplet to doublet energy transfer: improving organic light-emitting diodes with radicals

Emrys W. Evans^{2,3+}, Alexander J. Gillett²⁺, Qinying Gu², Junshuai Ding¹, Zhangwu Chen¹, Timothy J. H. Hele⁴, Richard H. Friend^{2*}, Feng Li^{1,2*}

¹State Key Laboratory of Supramolecular Structure and Materials, College of Chemistry, Jilin University, Qianjin Avenue 2699, Changchun, 130012, P. R. China

²Cavendish Laboratory, University of Cambridge, JJ Thomson Avenue, Cambridge, CB3 0HE, United Kingdom

³Department of Chemistry, Swansea University, Singleton Park, Swansea, SA2 8PP, United Kingdom

⁴Department of Chemistry, University College London, Christopher Ingold Building, London, WC1H 0AJ, United Kingdom

⁺denotes equal contribution

*e-mail correspondence to: rhf10@cam.ac.uk (RHF), lifeng01@jlu.edu.cn (FL)

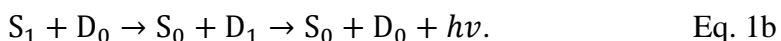
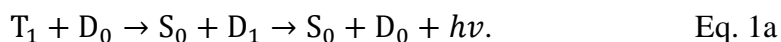
Contents

1. Theoretical considerations of energy transfer by FRET and Dexter mechanisms.....	23
The energy transfer system	23
Spin	24
Electronic interaction	26
2. Transient absorption (TA) studies of 4CzIPN and TTM-3PCz films.....	27
TA of 4CzIPN:CBP	27
TA of TTM-3PCz:CBP.....	29
TA of 4CzIPN:TTM-3PCz:CBP.....	30
3. Electroluminescence time dependence of 4CzIPN:TTM-3PCz:CBP OLEDs.....	31
4. Steady-state photoluminescence of 4CzIPN:TTM-3PCz:CBP film.....	32
5. Magneto-conductance studies of 4CzIPN:CBP and 4CzIPN:TTM-3PCz:CBP OLEDs.....	33

6. Temperature dependence on transient photoluminescence of 4CzIPN:CBP and 4CzIPN:TTM-3PCz:CBP films34

1. Theoretical considerations of energy transfer by FRET and Dexter mechanisms

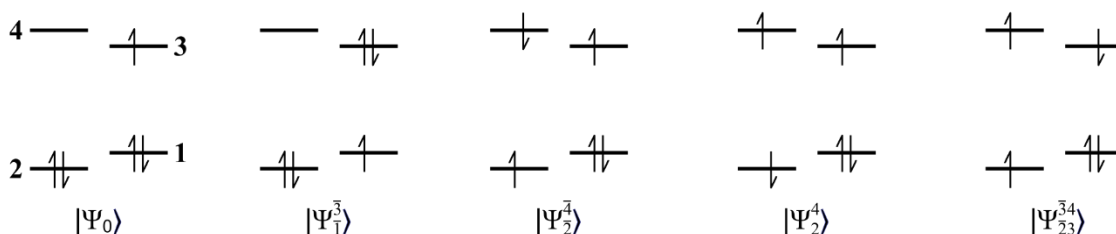
Here we consider the electronic structure algebra of the following energy transfer and emission processes:



In this section we demonstrate that both these processes are fully quantum mechanically spin-allowed (without requiring spin-orbit coupling) as they can conserve both total spin S and spin projection M_S .

The energy transfer system

We consider a minimal four (spatial) orbital, five-electron model that comprises: the HOMO of the radical energy acceptor, **A** (orbital 1); the SOMO of **A** (orbital 3); the HOMO of the energy donor, **D** (orbital 2); and the LUMO of **D** (orbital 4).



The electronic states considered are:

$$|\Psi_0\rangle = |1\bar{1}2\bar{2}3\rangle = |\mathbf{D}(S_0)\mathbf{A}(D_{0,+1/2})\rangle \quad \text{Eq. 2a}$$

$$|\Psi_1^3\rangle = |1\bar{3}2\bar{2}3\rangle = |\mathbf{D}(S_0)\mathbf{A}(D_{1,+1/2})\rangle \quad \text{Eq. 2b}$$

$$|\Psi_2^4\rangle = |1\bar{1}2\bar{4}3\rangle \quad \text{Eq. 2c}$$

$$|\Psi_2^4\rangle = |1\bar{1}4\bar{2}3\rangle \quad \text{Eq. 2d}$$

$$|\Psi_{23}^{\bar{3}4}\rangle = |1\bar{1}2\bar{3}4\rangle = |\mathbf{D}(T_{1,+1})\mathbf{A}(D_{0,-1/2})\rangle \quad \text{Eq. 2e}$$

where no bar indicates electron-spin ‘up’ and bar indicates electron-spin ‘down’.

We wish to identify these determinants in the basis of the S_0 , S_1 and T_1 electronic states of \mathbf{D} , and the D_0 and D_1 states of \mathbf{A} . This is already set out Eq. 2a, Eq. 2b and Eq. 2e. This can be achieved from Eq. 2c and Eq. 2d by taking linear combinations:

$$\frac{1}{\sqrt{2}}\left(|\Psi_{2}^{\bar{4}}\rangle + |\Psi_{2}^4\rangle\right) = |\mathbf{D}(S_1)\mathbf{A}(D_{0,+1/2})\rangle \quad \text{Eq. 3}$$

$$\frac{1}{\sqrt{2}}\left(|\Psi_{2}^{\bar{4}}\rangle - |\Psi_{2}^4\rangle\right) = |\mathbf{D}(T_{1,0})\mathbf{A}(D_{0,+1/2})\rangle. \quad \text{Eq. 4}$$

For states of non-zero spin (doublets and triplets) we have added a subscript index of the projection spin quantum number, M_S .

Spin

All determinants in Eq. 2 are eigenstates of the \hat{S}_z operator with eigenvalue, $M_S = + 1/2$. In addition, $|\Psi_0\rangle$ and $|\Psi_1^{\bar{3}}\rangle$ are eigenstates of the \hat{S}^2 operator with eigenvalue: $3/4 = 1/2(1 + 1/2)$ and are doublet-spin states. However the other three determinants are not eigenstates of \hat{S}^2 , and can be evaluated from three state basis in spin matrix:

$$\mathbf{S}^2 \mapsto \begin{pmatrix} 7/4 & -1 & -1 \\ -1 & 7/4 & +1 \\ -1 & +1 & 7/4 \end{pmatrix}. \quad \text{Eq. 5}$$

Eq. 5 has eigenvalues $15/4 = (3/2) \times (5/2)$, corresponding to a quartet, and $\frac{3}{4} = \frac{1}{2} \times \frac{3}{2}$ twice, corresponding to two doublets.

The quartet is uniquely defined as:

$$|Q\rangle = \sqrt{\frac{2}{3}}|\mathbf{D}(T_{1,0})\mathbf{A}(D_{0,+1/2})\rangle - \sqrt{\frac{1}{3}}|\mathbf{D}(T_{1,+1})\mathbf{A}(D_{0,-\frac{1}{2}})\rangle \mapsto \sqrt{\frac{1}{3}}\begin{pmatrix} +1 \\ -1 \\ -1 \end{pmatrix}, \quad \text{Eq. 6}$$

and the two doublet states can be chosen to be:

$$|D(a)\rangle = \sqrt{\frac{1}{3}}|\mathbf{D}(T_{1,0})\mathbf{A}(D_{0,+1/2})\rangle + \sqrt{\frac{2}{3}}|\mathbf{D}(T_{1,+1})\mathbf{A}(D_{0,-1/2})\rangle \mapsto \sqrt{\frac{1}{6}}\begin{pmatrix} +1 \\ -1 \\ +2 \end{pmatrix} \quad \text{Eq. 7}$$

$$|D(b)\rangle = |\mathbf{D}(S_1)\mathbf{A}(D_{0,+1/2})\rangle \mapsto \sqrt{\frac{1}{2}}\begin{pmatrix} +1 \\ +1 \\ 0 \end{pmatrix}. \quad \text{Eq. 8}$$

Note that $|\mathbf{D}(S_1)\mathbf{A}(D_{0,+1/2})\rangle$ is an eigenstate of \hat{S}^2 whereas $|\mathbf{D}(T_{1,0})\mathbf{A}(D_{0,+1/2})\rangle$ and $|\mathbf{D}(T_{1,+1})\mathbf{A}(D_{0,-1/2})\rangle$ are not. Although different linear combinations of the doublet eigenstates can be taken, it is possible to verify that the triplet-doublet determinants cannot be eigenstates of \hat{S}^2 .

Electronic interaction

We aim to find the interaction between the spin eigenstates $|Q\rangle$, $|D(a)\rangle$, $|D(b)\rangle$ and the emissive doublet state $|\Psi_1^{\bar{3}}\rangle = |1\bar{3}2\bar{2}3\rangle = |\mathbf{D}(S_0)\mathbf{A}(D_{1,+1/2})\rangle$. We find:

$$\langle \Psi_1^{\bar{3}} | \hat{H} | \Psi_2^{\bar{4}} \rangle = (13|24) - (12|34) \quad \text{Eq. 9}$$

$$\langle \Psi_1^{\bar{3}} | \hat{H} | \Psi_2^4 \rangle = (13|24) \quad \text{Eq. 10}$$

$$\langle \Psi_1^{\bar{3}} | \hat{H} | \Psi_{23}^{\bar{3}4} \rangle = -(12|34) \quad \text{Eq. 11}$$

where we have integrated out the spin contributions and written the integrals in chemists' notation (Szabo A, Ostlund NS. *Modern quantum chemistry: introduction to advanced electronic structure theory*, 2012).

$$(12|34) = \int d\mathbf{r}_1 \int d\mathbf{r}_2 \psi_1^*(\mathbf{r}_1) \psi_2(\mathbf{r}_1) \frac{1}{r_{12}} \psi_3^*(\mathbf{r}_2) \psi_4(\mathbf{r}_2)$$

where $\psi_2(\mathbf{r}_1)$ corresponds to the value of the wavefunction of orbital 2 at position \mathbf{r}_1 .

The integral (13|24) is a dipole-dipole (FRET) term at lowest order, whereas (12|34) is a Dexter electron-exchange term. From evaluating the $|Q\rangle$, $|D(a)\rangle$, $|D(b)\rangle$ terms we find:

$$\langle \Psi_1^{\bar{3}} | \hat{H} | Q \rangle = 0 \quad \text{Eq. 12}$$

$$\langle \Psi_1^{\bar{3}} | \hat{H} | D(a) \rangle = -\sqrt{\frac{3}{2}}(12|34) \quad \text{Eq. 13}$$

$$\langle \Psi_1^{\bar{3}} | \hat{H} | D(b) \rangle = \sqrt{2}(13|24) - \sqrt{\frac{1}{2}}(12|34) \quad \text{Eq. 14}$$

This means that $|\mathbf{D}(S_1)\mathbf{A}(D_{0,+1/2})\rangle$ and $|\mathbf{D}(S_0)\mathbf{A}(D_{1,+1/2})\rangle$ interact by both FRET and Dexter terms (with FRET term expected to dominate). There is no interaction between quartet state $|Q\rangle$ and $|\mathbf{D}(S_0)\mathbf{A}(D_{1,+1/2})\rangle$, as expected on grounds of spin conservation, and the total triplet-doublet (D_1) pair interacts only via a Dexter-type term.

2. Transient absorption (TA) studies of 4CzIPN and TTM-3PCz films

TA of 4CzIPN:CBP

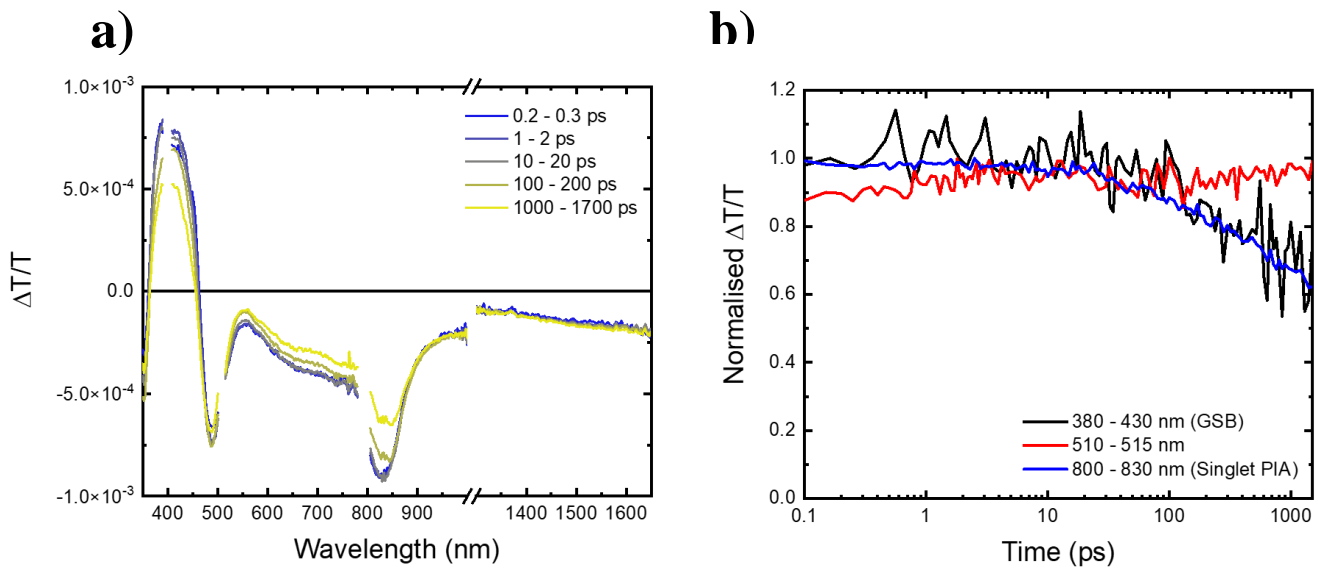


Figure S1. Short-time TA of 4CzIPN:CBP with 400 nm excitation. a) $\Delta T/T$ timeslices of 4CzIPN:CBP (0.25:0.75) films with 400 nm excitation at $89.1 \mu\text{J}/\text{cm}^2$ fluence, from 0.2-0.3 ps to 1000-1700 ps. b) Normalised $\Delta T/T$ kinetic profiles of 380-430 nm (ground state bleach, GSB); 510-515 nm and 800-830 nm that are photoinduced absorption (PIA) signals we assign to 4CzIPN S_1 .

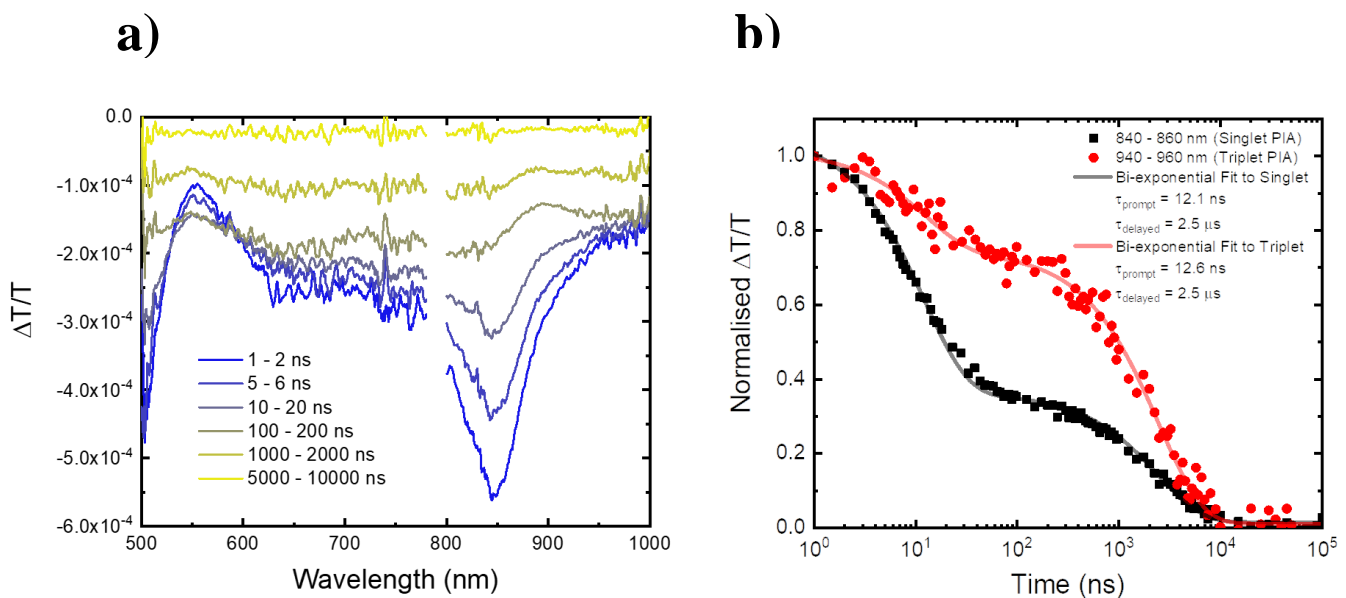


Figure S2. Long-time TA of 4CzIPN:CBP with 355 nm excitation. a) $\Delta T/T$ timeslices of 4CzIPN:CBP (0.25:0.75) films with 355 nm excitation at 17.0 $\mu\text{J}/\text{cm}^2$ fluence, from 1-2 ns to 5000-10000 ns. b) Normalised $\Delta T/T$ kinetic profiles of 840-860 nm (we assign to 4CzIPN S_1 PIA from Fig. S1a); and 940-960 nm (here we assign to 4CzIPN T_1 PIA).

TA of TTM-3PCz:CBP

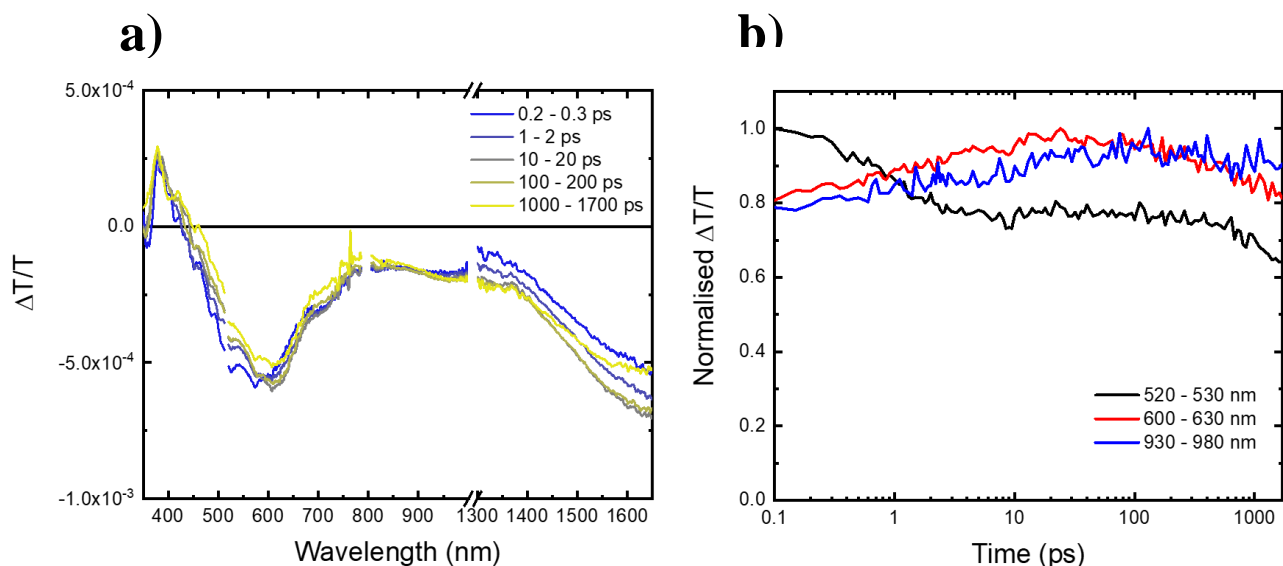


Figure S3. Short-time TA of TTM-3PCz:CBP with 400 nm excitation. a) $\Delta T/T$ timeslices of TTM-3PCz:CBP (0.03:0.97) films with 400 nm excitation at $89.1 \mu\text{J}/\text{cm}^2$ fluence, from 0.2-0.3 ps to 1000-1700 ps. b) Normalised $\Delta T/T$ kinetic profiles of 520-530 nm; 600-630 nm and 930-980 nm that are photoinduced absorption (PIA) signals we assign to excited states of TTM-3PCz.

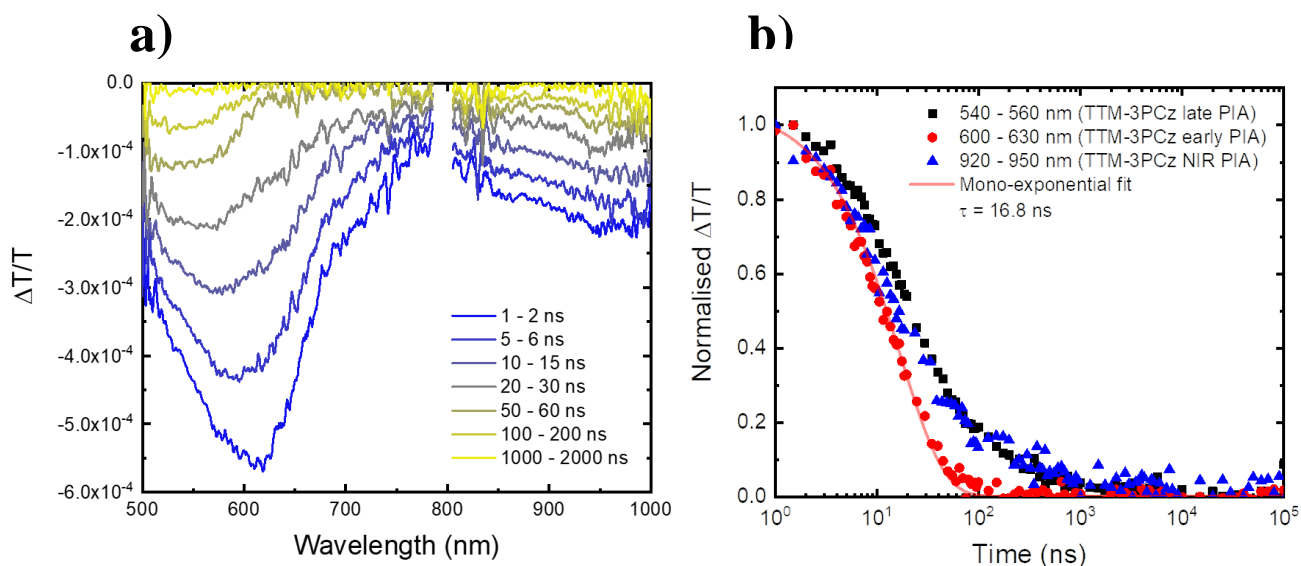


Figure S4. Long-time TA of TTM-3PCz:CBP with 355 nm excitation. a) $\Delta T/T$ timeslices of TTM-3PCz:CBP (0.03:0.97) films with 355 nm excitation at $3.85 \mu\text{J}/\text{cm}^2$ fluence, from 1-2 ns to 1000-2000 ns. b) Normalised $\Delta T/T$ kinetic profiles of 540-560 nm (TTM-3PCz, late PIA from short-time TA); 600-630 nm (TTM-3PCz, early PIA from short-time TA) and 920-950 nm (TTM-3PCz, near-infrared wavelength PIA).

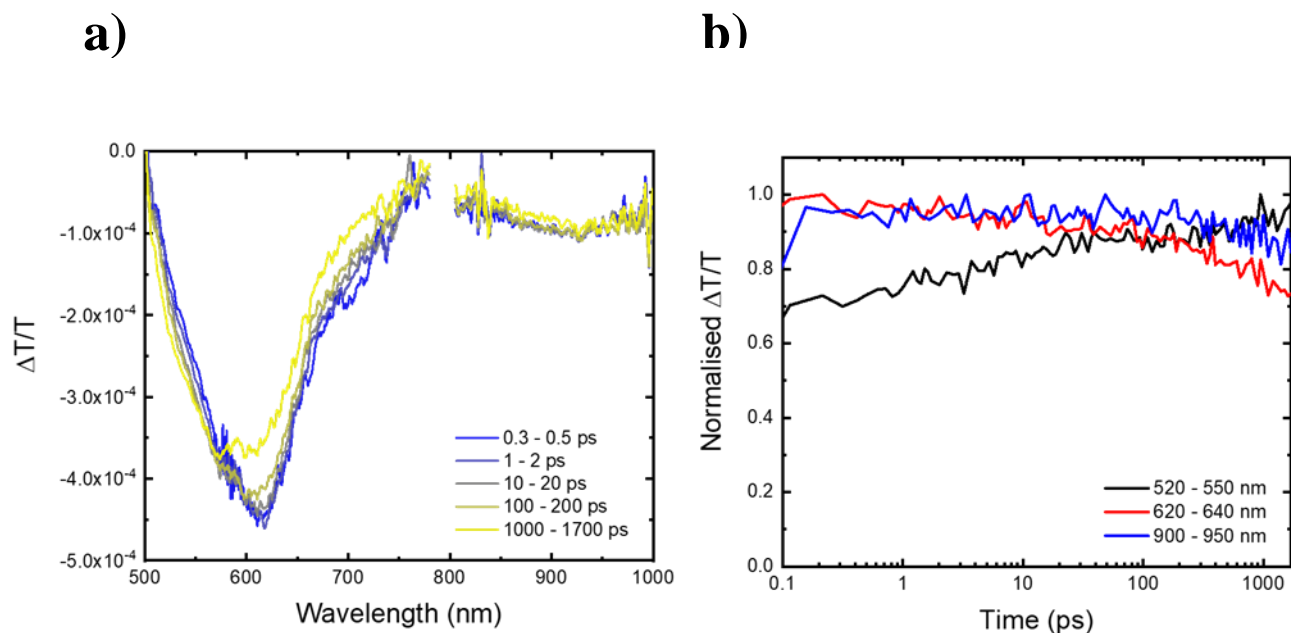


Figure S5. Short-time TA of TTM-3PCz:CBP with 600 nm excitation. a) $\Delta T/T$ timeslices of TTM-3PCz:CBP (0.03:0.97) films with 600 nm excitation at $131.3 \mu\text{J}/\text{cm}^2$ fluence, from 0.3-0.5 ps to 1000-1700 ps. b) Normalised $\Delta T/T$ kinetic profiles of 520-550 nm; 620-640 nm and 900-950 nm that are photoinduced absorption (PIA) signals we assign to excited states of TTM-3PCz.

TA of 4CzIPN:TTM-3PCz:CBP

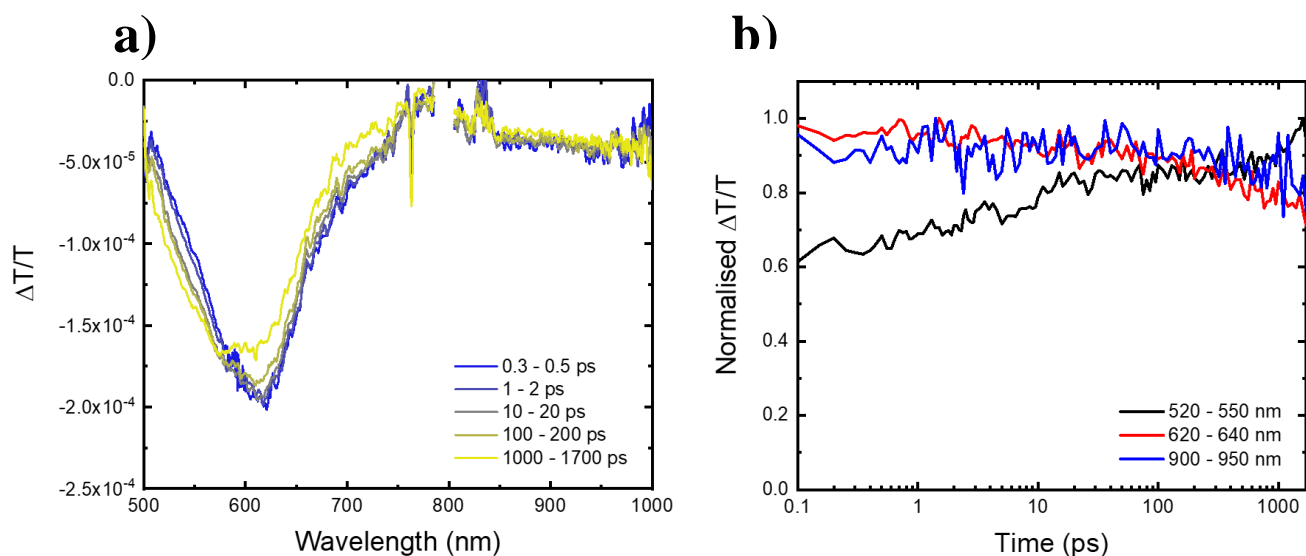


Figure S6. Short-time TA of 4CzIPN:TTM-3PCz:CBP with 600 nm excitation. a) $\Delta T/T$ timeslices of 4CzIPN:TTM-3PCz:CBP (0.25:0.03:0.72) films with 600 nm excitation at $131.3 \mu\text{J}/\text{cm}^2$ fluence, from 0.3-0.5 ps to 1000-1700 ps. b) Normalised $\Delta T/T$ kinetic profiles of 520-550 nm; 620-640 nm and 900-950 nm that are photoinduced absorption (PIA) signals we assign to excited states of TTM-3PCz. Comparison of TA for 4CzIPN:TTM-3PCz:CBP and TTM-3PCz:CBP films with 600 nm excitation (Fig. S5 and S6) shows that D_1 excitons formed for TTM-3PCz does not interact with 4CzIPN.

3. Electroluminescence time dependence of 4CzIPN:TTM-3PCz:CBP

OLEDs

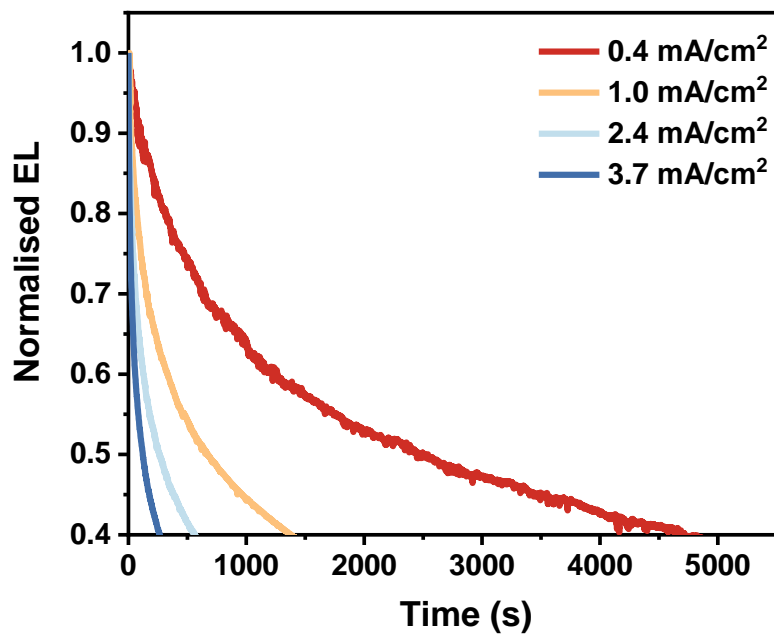


Figure S7. Normalised EL time dependence of 4CzIPN:TTM-3PCz:CBP OLEDs with fixed current density values. The device half-time T_{50} values were found to be: 42 min at $0.4 \text{ mA}/\text{cm}^2$; 10.5 min at $1.0 \text{ mA}/\text{cm}^2$; 4.5 min at $2.4 \text{ mA}/\text{cm}^2$; 2 min at $3.7 \text{ mA}/\text{cm}^2$ (T_{50} = time for luminance to fall to half of initial value under constant current density operation).

4. Steady-state photoluminescence of 4CzIPN:TTM-3PCz:CBP film

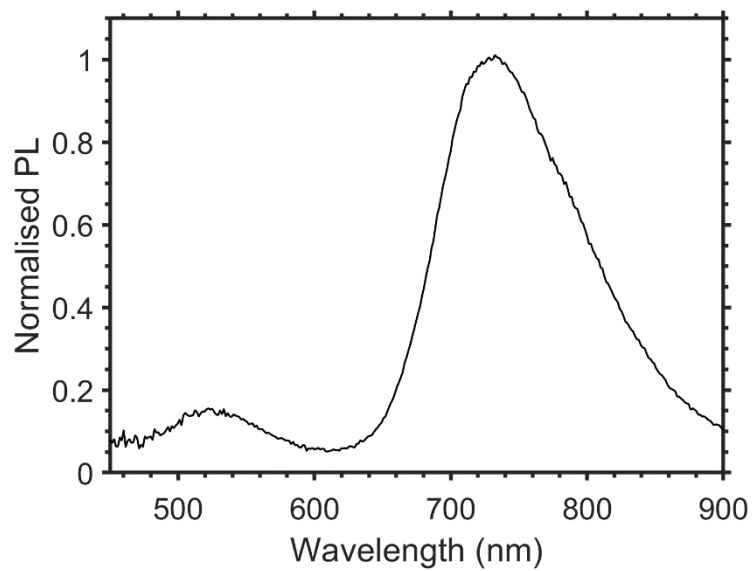


Figure S8. Photoluminescence of 4CzIPN:TTM-3PCz:CBP film. Steady-state PL of 4CzIPN:TTM-3PCz:CBP (0.25:0.03:0.72) from 405 nm excitation.

5. Magneto-conductance studies of 4CzIPN:CBP and 4CzIPN:TTM-3PCz:CBP OLEDs

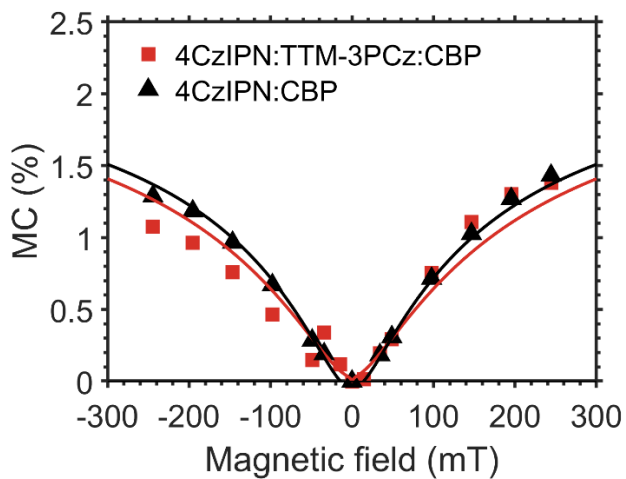


Figure S9. Magneto-conductance (MC) studies of 4CzIPN:CBP, 4CzIPN:TTM-3PCz:CBP OLEDs. Studied OLEDs were fabricated according to Fig. 4a, main text with emissive layers (30 nm): 4CzIPN:TTM-3PCz:CBP (0.25:0.03:0.72), red squares; 4CzIPN:CBP (0.25:0.75), black triangles. Data collected simultaneously with magneto-electroluminescence from Fig. 4f.

6. Temperature dependence on transient photoluminescence of 4CzIPN:CBP and 4CzIPN:TTM-3PCz:CBP films

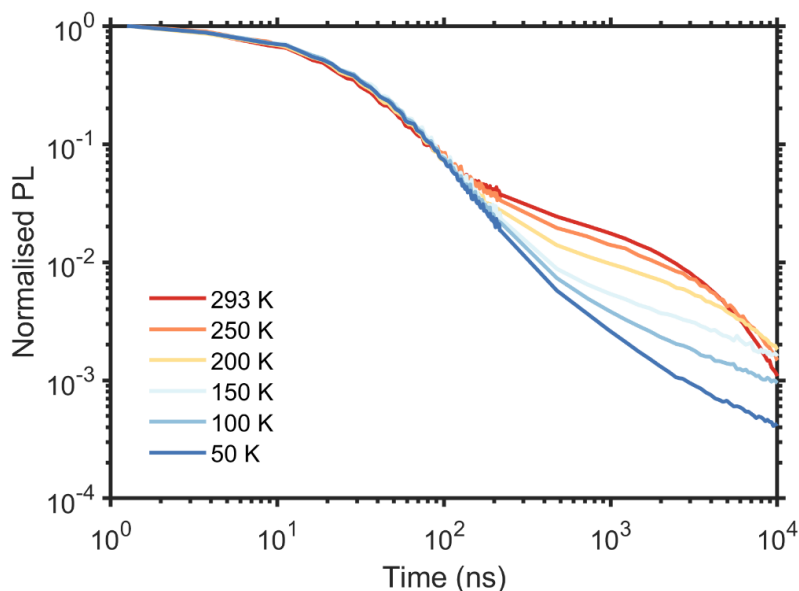


Figure S10. Temperature dependence of transient photoluminescence profiles for 4CzIPN:CBP film for 4CzIPN emission. Transient PL profiles for nano-to-micro-second time ranges (with 400 nm excitation at $5 \mu\text{J}/\text{cm}^2$) of 4CzIPN:CBP (0.25:0.75) at various temperatures from 50 to 293 K, averaged for total 4CzIPN emission (450-650 nm range).

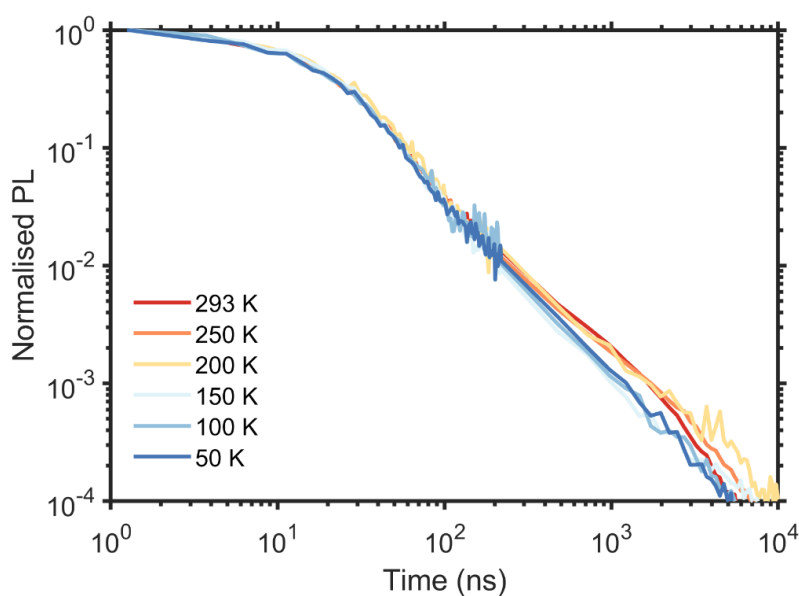


Figure S11. Temperature dependence of transient photoluminescence profiles for 4CzIPN:TTM-3PCz:CBP film for TTM-3PCz emission. Transient PL profiles for nano-to-micro-second time ranges

(with 400 nm excitation at 5 $\mu\text{J}/\text{cm}^2$) of 4CzIPN:TTM-3PCz:CBP (0.25:0.03:0.72) at various temperatures from 50 to 293 K, averaged for TTM-3PCz emission (700-800 nm range).